Applied Surface Science 330 (2015) 10–19

Contents lists available at ScienceDirect

Applied Surface Science

journal homepage: www.elsevier.com/locate/apsusc

Structural rearrangement of mesostructured silica nanoparticles incorporated with ZnO catalyst and its photoactivity: Effect of alkaline aqueous electrolyte concentration

N.W.C. Jusoh[a], A.A. Jalil[a,b,*], S. Triwahyono[c], A.H. Karim[c], N.F. Salleh[a], N.H.R. Annuar[c], N.F. Jaafar[c], M.L. Firmansyah[c], R.R. Mukti[d], M.W. Ali[a,b]

[a] Department of Chemical Engineering, Faculty of Chemical Engineering, Universiti Teknologi Malaysia, 81310 UTM Johor Bahru, Johor, Malaysia
[b] Institute of Hydrogen Economy, Universiti Teknologi Malaysia, 81310 UTM Johor Bahru, Johor, Malaysia
[c] Department of Chemistry, Faculty of Science, Universiti Teknologi Malaysia, 81310 UTM Johor Bahru, Johor, Malaysia
[d] Division of Inorganic and Physical Chemistry, Faculty of Mathematics and Natural Science, Institut Teknologi Bandung, Jl Ganesha No 10, Bandung 40132, Indonesia

ARTICLE INFO

Article history:
Received 2 September 2014
Received in revised form
12 November 2014
Accepted 30 December 2014
Available online 5 January 2015

Keywords:
Structural rearrangement
Alkaline electrolyte
Mesostructured silica nanoparticles
Zinc oxide
Photodecolorization

ABSTRACT

ZnO-incorporated mesostructured silica nanoparticles (MSN) catalysts (ZM) were prepared by the introduction of Zn ions into the framework of MSN via a simple electrochemical system in the presence of various concentrations of NH_4OH aqueous solution. The physicochemical properties of the catalysts were studied by XRD, ^{29}Si MAS NMR, nitrogen adsorption–desorption, FE-SEM, TEM, FTIR, and photoluminescence spectroscopy. Characterization results demonstrated that the alkaline aqueous electrolyte simply generated abundant silanol groups on the surface of the catalysts as a consequence of desilication to form the hierarchical-like structure of the MSN. Subsequent restructuring of the silica network by the creation of oxygen vacancies and formation of Si–O–Zn during the electrolysis, as well as formation of new Si–O–Si bonds during calcination seemed to be the main factors that enhanced the catalytic performance of photodecolorization of methyl orange. A ZM prepared in the presence of 1.0 M NH_4OH (ZM-1.0) was determined to be the most effective catalyst. The catalyst displays a higher first-order kinetics rate of $3.87 \times 10^{-1}\ h^{-1}$ than unsupported ZnO ($1.13 \times 10^{-1}\ h^{-1}$) that prepared under the same conditions in the absence of MSN. The experiment on effect of scavengers showed that hydroxyl radicals generated from the three main sources; reduced O_2 at the conduction band, decomposed water at the valence band and irradiated H_2O_2 in the solution, are key factors that influenced the reaction. It is also noted that the recycled ZM-1.0 catalyst maintained its activity up to five runs without serious catalyst deactivation.

1. Introduction

Heterogeneous photocatalysis is a promising technology for the removal of dyes from wastewater [1]. It has great potential as an environmental friendly, low cost, and sustainable technology. Various semiconductors, including TiO_2, Fe_2O_3, ZnO, and CuO, were used as photocatalysts because of their ability to decolorize dye-containing wastewater [2,3]. Of the various semiconductor materials, ZnO stands out due to its properties and wide applications. ZnO features a band gap of 3.37 eV, efficient absorption in a larger fraction of solar energy, and has a low cost. Therefore, it is considered as a favorable semiconductor with potential uses in photocatalysis [4]. It has been demonstrated that the photocatalytic activity of semiconductors are correlated to the morphology, crystalline phase, porosity, and surface area of the materials [5]. Additionally, the surface defect sites of the catalyst are thought to be a main factor affecting the electron–hole recombination process during photocatalysis [6]. To achieve the target, many researchers have tried to improve the photocatalytic activity of the semiconductors by using mesoporous materials as the support.

Recently, studies on the synthesis of mesoporous silica (MS) materials have received much attention and the field has advanced rapidly. The MS materials, such as MCM-41 and SBA-15, have been extensively investigated due to their unique properties [7]. In response to this, mesostructured silica nanoparticles (MSN) have become increasingly important because of their high surface area,

* Corresponding author at: Department of Chemical Engineering, Faculty of Chemical Engineering, Universiti Teknologi Malaysia, 81310 UTM Johor Bahru, Johor, Malaysia. Tel.: +60 7 5535581; fax: +60 7 5588166.
E-mail address: aishah@cheme.utm.my (A.A. Jalil).

http://dx.doi.org/10.1016/j.apsusc.2014.12.192
0169-4332/

highly uniform pore distribution, tunable pore size, and unique hosting properties. Previously, we reported the great potential of MSN as a support material in ibuprofen delivery [8], CO_2 methanation [9], cumene cracking [10], and adsorption of organic pollutant [11].

Although the catalytic ability of the semiconductors could be enhanced by using these mesoporous materials, many problems still arise. At times, the pores in these materials are not large enough to help the fast internal diffusion and mass transfer [12]. It is believed that the modification of mesoporous material to form hierarchical structures is a beneficial approach to improve the properties and effectiveness of the catalysts without changing the chemical composition of the materials [13]. Miao et al. reported an efficient catalytic ability of Fe_2O_3 supported on hierarchically porous silica (Fe_2O_3/HPS) for the degradation of Orange II due to the excellent pore structure of HPS [14]. Based on this information, many researchers have pursued the creation of hierarchically structure materials.

In particular, desilication by alkaline treatment was shown to be an effective way to prepare hierarchical porous materials [15]. This selective removal of siliceous species has become a widely used top-down method. The studies on the alkali-treatment of zeolites, which used Na_2CO_3 or NaOH solution, showed that selective removal of the siliceous species from the zeolite framework occurs without changes to the zeolitic structure [16,17]. However, these conventional methods required high temperature, longer reaction times, and included somewhat troublesome steps [18,19]. We have previously reported the dealumination of the aluminosilicate framework of zeolites by a simple electrochemical method under nitrogen atmosphere accompanied by isomorphous substitution of metal ions (Zr^{4+}, Fe^{3+}, and Zn^{2+}). These metal-supported catalysts led to enhanced photodecolorization of various dyes [20,21]. On the other hand, we also reported a sequential desilication–isomorphous substitution method to prepare mesostructured silica nanoparticles loaded with ZnO [22]. The dealumination and desilication were achieved successfully by electrolysis under mild conditions without using strong acidic conditions, hydrothermal treatment, higher temperature, and/or reactive compounds [23]. Therefore, in this study, we further explored the possible preparation of hierarchically ordered structures of MSN using the similar electrochemical system by altering the conditions of electrolyte. We found that by controlling the weak alkaline concentration, a different degree of desilication was achieved and subsequent rearrangement of the silica network during the electrolysis as well as calcination enhanced the catalytic performance for photodecolorization of methyl orange dye. The catalysts were characterized by XRD, ^{29}Si MAS NMR, nitrogen adsorption–desorption, FE-SEM, TEM, FTIR, and photoluminescence. A proposed structure and involvement of both Zn and NH_4OH solution in the silica structural rearrangement were elucidated in detail from the characterization results. A proposed mechanism for photodecolorization, as well as kinetics studies, is also discussed.

2. Experimental

2.1. Materials

All chemicals were reagent grade and used without further purification. For preparation of mesostructured silica nanoparticles (MSN), cetyltrimethylammonium bromide (CTAB), ethylene glycol (EG), tetraethyl orthosilicate (TEOS), 3-aminopropyl triethoxysilane (APTES) as surfactant, co-solvent, silica source and pore expander, respectively were purchase from MERCK Sdn. Bhd., Malaysia. Ammonium hydroxide solution (NH_4OH) was obtained from QRec, Malaysia. The platinum and zinc plates (99.99% purity) which used in the electrolysis were obtained from Nilaco Metal, Japan. The supported electrolyte, tetraethylammonium perchlorate (TEAP) was synthesized in accordance with the procedure reported in the literature [24]. In the photocatalytic experiment, sodium hydroxide (NaOH) and hydrochloric acid (HCl) were used to adjust the pH of distilled water for preparation of methyl orange (MO) solution. These materials were also supplied from MERCK Sdn. Bhd., Malaysia. The distilled water was used throughout in the experiment.

2.2. Catalyst preparation

The mesostructured silica nanoparticles (MSN) were prepared by a co-condensation and sol–gel method as reported in previous literature [11], corresponding to the mole composition of 0.0032:0.2:0.2:0.1 for CTAB, EG, NH_4OH and water, respectively. The mixture was stirred vigorously for about 30 min with heating. Then 1.2 mmol TEOS and 1 mmol APTES were added to the clear mixture to give a white suspension solution. This solution was then stirred for another 2 h, and the samples were collected by centrifugation. The synthesized MSN were dried at 333 K and calcined at 823 K for 3 h to remove the surfactant.

The ZnO/MSN catalysts were prepared according to previous report protocol with some modification [22,25,26]. A 10 mL distilled water with different amount of NH_4OH (0, 0.5, 1.0 and 2.0 M) were added into 1 g of MSN in an open system electrolysis cell fitted with a magnetic stirrer and a platinum plate cathode ($2 \times 2\,cm^2$) facing a zinc plate anode ($2 \times 2\,cm^2$). As a supporting electrolyte, 0.1 M TEAP were added into the mixture. The electrolysis undergo in a constant current of $120\,mA\,cm^{-2}$ and 0 °C under air atmosphere. 5 min 26 s was required to load 5 wt% of the ZnO onto the MSN as calculated by the Faraday's law as follows,

$$t = \left(\frac{F}{I}\right)(z \times n) \quad (1)$$

where t is a total time for the constant current applied (s); F is a Faraday constant, 96,486 C mol^{-1}; I is an electric current applied; z is a valency number of ions of substances (electrons transferred per ion); and n is an amount of substance (number of moles, liberated $n = m/M$). The Zn plate was weighed before and after the electrolysis to confirm the exact amount of Zn.

After electrolysis, the obtained mixture was impregnated and dried at 383 K for 12 h before being calcined at 823 K for 3 h to yield a white powder catalyst which is ready for a characterization. The catalysts were denoted as ZM-*X*, where *X* is a molarity of the NH_4OH used in the synthesis.

2.3. Characterization

The crystalline structures of the catalysts were confirmed by X-ray powder diffraction (XRD) analysis carried out at room temperature using D8 ADVANCE Bruker X-ray diffractometer using Cu Kα radiation at a 2θ angle ranging from 2° to 10°. The phases were identified with the aid of the Joint Committee on Powder Diffraction Standards (JCPDS) files.

The textural properties (i.e., specific surface area and pore volume) were determined from nitrogen physisorption at 77 K using a Beckman Coulter SA 3100 surface area analyzer. The samples were outgassed at 573 K for 1 h prior to the analysis. Specific surface area (S_{BET}) values were calculated from the BET isotherm plots, while the total pore volume and pore size distributions were calculated using Non-Local Density Functional Theory (NLDFT) method from the isotherm. The morphological properties of the catalysts were examined by field emission scanning electron microscopy (FESEM) (JSM-6300F FESEM) and transmission electron microscopy (TEM).

Fourier Transform Infrared (FT-IR) measurements were carried out with Perkin-Elmer Spectrum GX FTIR Spectrometer using the KBr method with a scan range of 400–4000 cm^{-1}. IR evacuated was also performed by a self-supported wafer placed in an in-situ stainless steel IR cell with CaF_2 windows. The cell was heated at 673 K for 1 h to activate the catalysts and the spectra were recorded at room temperature. In order to compare the surface coverage of the adsorbed species between different wafer thicknesses, all spectra were normalized using the overtone and combination vibrations between 2100 and 1550 cm^{-1} after activation.

The photoluminescence (PL) analysis was performed using HORIBA Jobin Yvon with excitation energy of 325 nm to study the electronic structure, optical and photochemical properties of semiconductor materials, by which information such as surface oxygen vacancies and defects can be obtained.

The nuclear magnetic resonance measurements were carried out using ^{29}Si magic angle spinning nuclear magnetic resonance (MASNMR) Spectroscopy to determine the chemical status in the silica framework of the catalysts. The measurement was performed at room temperature on a Bruker Solid NMR (JEOL 400 MHz) spectrometer using tetramethylsilane (TMS) as an external reference. The spectra were recorded using 4 μs radio frequency pulses, a recycle delay of 60 s and spinning rate of 7 kHz using a 4 mm zirconia sample rotor.

2.4. Photocatalytic testing

The photoactivities of the catalysts were tested for decolorization of an aqueous solution of MO dye in a batch reactor fixed with UV lamp (4 × 9 W; 365 nm emission) and a cooling system. The photocatalytic testing was performed using 1 g L^{-1} of catalyst added to the MO solution with a concentration of 3.06×10^{-2} mM and initial pH of 2. The solution was stirred for 1 h in a dark to achieve adsorption–desorption equilibrium. Prior to photocatalytic measurement, the reaction was carried out for another 8 h under light irradiation with the addition of 3 wt% H_2O_2 under continuous stirring. The concentration of MO dye in the solution before irradiation was used as the initial value for the MO decolorization measurements. Then the samples were collected at regular interval of 1 h and centrifuged in a Hettich Zentrifugen Micro 120 at 75,000 rpm for 10 min before being analyzed by UV–vis spectrophotometer (Thermo Scientific Genesys10uv Scanning) for the residual concentration of MO. To ensure the accuracy, each set of experiments was performed three times. The MO decolorization was measured at the maximum adsorption peak at 506 nm.

The effect of different scavengers on photocatalytic performance was also evaluated using isopropanol (IP), sodium oxalate (SO), benzyl chloride (BC) and kalium iodide (KI). An amount of 0.65 mol L^{-1} of IP, SO, BC or KI was added to the system before subjected to irradiation. Then, the sample was collected and analyzed using the same procedure as mention above.

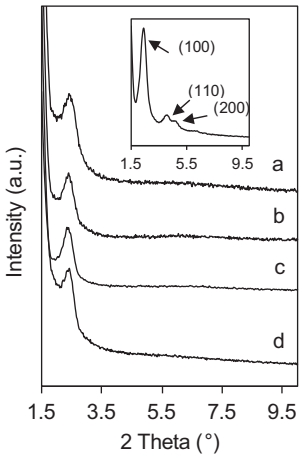

Fig. 1. Small-angle XRD patterns of ZM catalysts prepared by different amounts of NH_4OH (a) ZM-0 (b) ZM-0.5 (c) ZM-1.0 and (d) ZM-2.0. Inset figure shows XRD pattern of MSN.

3. Result and discussion

3.1. Characterization of catalysts

3.1.1. Structural studies

The structure of ZnO/MSN (ZM) catalysts prepared with different amounts of NH_4OH were examined by XRD with a small-angle pattern in the range of $2\theta = 1.5–10^\circ$ (Fig. 1). The inset figure shows the diffractogram of bare MSN, which indexed to a *p6mm* hexagonal structure of mesoporous silica with three main diffraction peaks at $2\theta = 2.39$, 4.05, and 4.71° relative to the (1 0 0), (1 1 0), and (2 0 0) reflections, respectively [22]. The (1 0 0) peak decreased considerably, while the (1 1 0) and (2 0 0) peaks eliminated when Zn and NH_4OH were introduced into the MSN (Fig. 1a–d), demonstrating the essential role of both species in the silica order rearrangement. A desilication might have occurred in the silica framework due to the presence of ammonium salt and/or alkaline solution during the electrolysis [27]. For the ZM-0 sample (Fig. 1a), the Zn ions may be isomorphously substituted following desilication, which led to perturbation of the silica framework and decreased the intensity of the (1 0 0) peak [20–22]. A similar diffractogram was reported by Li et al., in which the peaks for SBA-15 became less pronounce after the loading with TiO_2 [28]. There was no ZnO characteristic

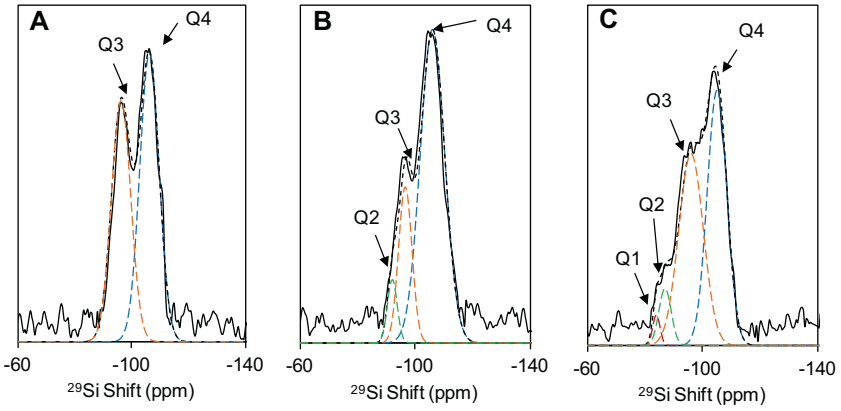

Fig. 2. ^{29}Si MAS NMR spectra of (A) MSN (B) ZM-0 and (C) ZM-2.0 catalysts.

peak in the high angle of the XRD pattern (figure not shown), suggested that ZnO might be in the framework or highly dispersed on the surface of MSN. Occasionally, the presence of diminutive metals could not be detected by XRD as similar phenomenon was reported when 8 wt% Fe was loaded onto MCM-41 [29]. The intensity of the (1 0 0) peak seemed to be slightly increased by the addition of 1.0 M NH_4OH (Fig. 1c), thus suggesting a possible improvement in the silica network. However, increasing NH_4OH to 2.0 M (Fig. 1d) reduced the peak intensity, showing the limitation in the amount of added base.

Next, the catalysts were further studied by ^{29}Si MAS NMR analysis. Fig. 2 shows a bare MSN and ZM catalysts spectra deconvolved with Gaussian fitting. The bare MSN shows an intense signal at −107 and −96 ppm, which is the silicon atoms at the Q4 site $(\equiv SiO)_4Si$ and Q3 site $(\equiv SiO)_3Si$, respectively (Fig. 2A) [10]. The introduction of Zn into MSN appeared to reduce the amount of Q3, while slightly increasing the amount of Q4 (Fig. 2B). A shoulder peak developed between −95 and −90 ppm, indicating the possible formation of a Q2 site $(\equiv SiO)_2Si$. Thus, the desilication could have occurred during the electrolysis accompanied by either isomorphous substitution of Zn ions with Si in the framework or leaving abundant silanol nests [22]. A signal corresponding to the Q1 site $(\equiv SiO)_1Si$ was also observed for the catalyst prepared in the presence of 2.0 M NH_4OH (ZM-2.0; Fig. 2C). This also verified that more desilication took place during the alkaline treatment and produced extra Si–O–Zn bonds or Si–O–H groups. A similar result was reported by Lihitkar et al., who showed that the Q2 site signal was observed for ZnO loaded on mesoporous silica and was due to the presence of the Si–O–Zn bond [30].

3.1.2. Morphological studies

The morphology related to the overall shape and size of the bare MSN and ZM-1.0 catalysts was illustrated by a field emission scanning electron microscopy (FE-SEM) and transmission electron microscopy (TEM), and the results are shown in Fig. 3. Due to the potential improvement in the silica network as demonstrated by the XRD result, the ZM-1.0 was chosen as a representative catalyst for this analysis. The spherical shape of the bare MSN, which had an average diameter of 100 nm (Fig. 3A), was slightly reduced and less aggregated when the ZnO and NH_4OH were introduced (Fig. 3B). The TEM image revealed that the bare MSN exhibited uniform and well oriented hexagonal pores, which represents a typical nanosized mesoporous silica (Fig. 3C) [11]. There were some distinct bright spots within the single crystal in Fig. 3D–F, thus demonstrating the hierarchical-like structure of the mesopores, which were generated by the possible desilication after alkaline treatment with the NH_4OH solution. On the other hand, the dark spots represented the existence of incorporated ZnO nanoparticles. This was confirmed by the fast Fourier transform (FFT) pattern, shown in the inset Fig. 3E, which exhibited the hexagonal diffraction spots of ZnO with the wurtzite structure [31]. Thus, in conjunction with the absence of peaks corresponding to wurtzite ZnO phase in the XRD pattern of ZM-0 ~ ZM-2.0, we believe that the ZnO nanoparticles were well dispersed in the mesopores of MSN [32].

3.1.3. Study of textural properties

The adsorption–desorption isotherms of N_2 were used to study the changes of the pore structure of ZM catalysts upon addition of different amounts of NH_4OH solution, and the results are shown in Fig. 4. A summary of the corresponding textural properties of the catalysts is shown in Table 1. As shown in Fig. 4A, a type IV isotherm curve and H1 hysteresis loop, which classification of highly uniform cylindrical pores, was observed for the bare MSN. A remarkable two steps of capillary condensation were observed, with the first step at $P/P_o = 0.3$ and the second step at higher partial pressure ($P/P_o = 0.9$), which were assigned to intraparticle and interparticle mesopores, respectively [9,33]. Based on the red reference line, Fig. 4B shows that the intraparticle pores of the MSN were drastically reduced and consequently decreased the pore volume when Zn was added to prepare the ZM-0. Table 1 shows that the surface area of pure MSN decreased considerably from 1137 to 658 $m^2\,g^{-1}$ and the pore volume decreased from 1.11 to 0.656 $mL\,g^{-1}$. These results implied the perturbation of silica network by the possible isomorphous substitution of Si with the larger Zn ions [30]. In addition, from the NLDHT pore width distribution of the catalysts shown in Fig. 4F, we observed that the high intensity of the bare MSN peak decreased sharply upon the addition of Zn, verifying the pore blockage effect due to the presence of the new metal ions. However, the addition of NH_4OH to the system seemed to slightly increase the porosity and interparticle pores of the catalyst (Fig. 4C). The interparticle pores continued to increase with increasing amounts of NH_4OH up to 1.0 M (Fig. 4D), indicating an improvement in the silica network, which may be associated with the possible formation of a hierarchical-like structure of the MSN [34]. This result was in agreement with the XRD data, which demonstrated the increment in intensity of the (1 0 0) peak of ZM-1.0 when compared to ZM-0.5. It was anticipated that the base treatment would trigger partial desilication, which can introduce a large number of intraparticle mesopores and allow for the incorporation of zinc ions into the mesopores during the electrolysis. The results shown in Table 1 confirmed the increase in surface area and pore volume of ZM-1.0 when compared to ZM-0.5. Similar structural enhancement was reported in the synthesis of the mesoporous ZSM-5 zeolite incorporating ZnO loading in the presence of NaOH by the wet impregnation method [31]. Fig. 4F also shows that the addition of NH_4OH up to 1.0 M almost retained the pattern of pore width of the ZM catalysts. Nevertheless, further addition of NH_4OH up to 2.0 M seems eliminated the intraparticle pores at 3.24 nm, while the interparticle pores at 4.41 nm were almost unchanged and formation of higher pores are observed at the range of 5.5–10.0 nm. The higher concentration of alkaline solution might collapse the smaller pore walls which then reduced the pore volume (Table 1) and increased the porosity (Fig. 4E). Similar phenomenon was reported on desilication of ZSM-5 with NaOH solution, in which the increasing concentration of NaOH increased the fraction of mesoporosity and decreased the micropore volume of zeolites [35].

Table 1
Textural properties and kinetics decolorization parameters of the catalysts.

Catalyst	Surface area ($m^2\,g^{-1}$)	Pore volume ($mL\,g^{-1}$)	$k^a \times 10^{-1}$ (h^{-1})	$k^b \times 10^{-3}$ ($h^{-1}/m^2\,g^{-1}$)
MSN	1137	1.11	0.13	0.011
ZM-0	658	0.656	2.14	0.324
ZM-0.5	643	0.712	2.85	0.443
ZM-1.0	771	0.824	3.87	0.501
ZM-2.0	467	0.671	1.49	0.318

[a] First-order rate constant.
[b] The *k* values were normalized with the surface area.

3.1.4. Vibrational spectroscopy

Fig. 5A shows the FTIR spectra of MSN and ZM catalysts in the region between 4000 and 400 cm^{-1}. All of the catalysts exhibited bands attributed to –OH stretching (3452 cm^{-1}), water molecules retained by siliceous materials (1635 cm^{-1}), Si–O–Si asymmetric stretching (1084 cm^{-1}), external Si–OH groups (966 cm^{-1}), Si–O–Si symmetric stretching (796 cm^{-1}), and Si–O–Si bending (460 cm^{-1}). In order to ascertain the desilication and/or isomorphous substitution in the silica framework for determining the authentic structure of the catalysts, the percentage of intensity change in the related band was calculated based on the intensity of the bare MSN. Four bands (1084, 966, 796, and 460 cm^{-1}) were selected, and the results are illustrated in Fig. 5B. The Si–O–Si bands at 796 and 460 cm^{-1}

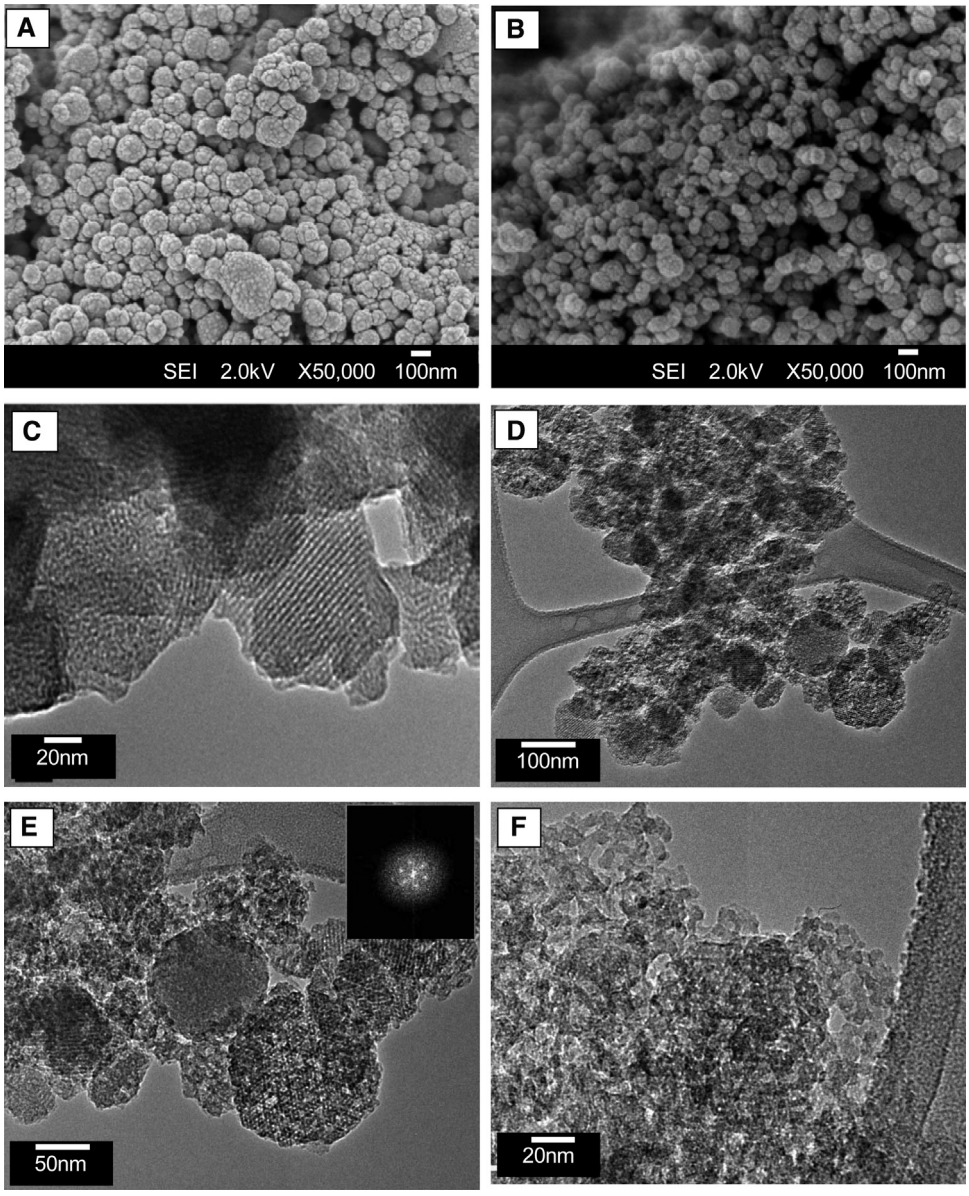

Fig. 3. FESEM and TEM images of (A, C) MSN and (B, D, E, F) ZM-1.0 catalysts.

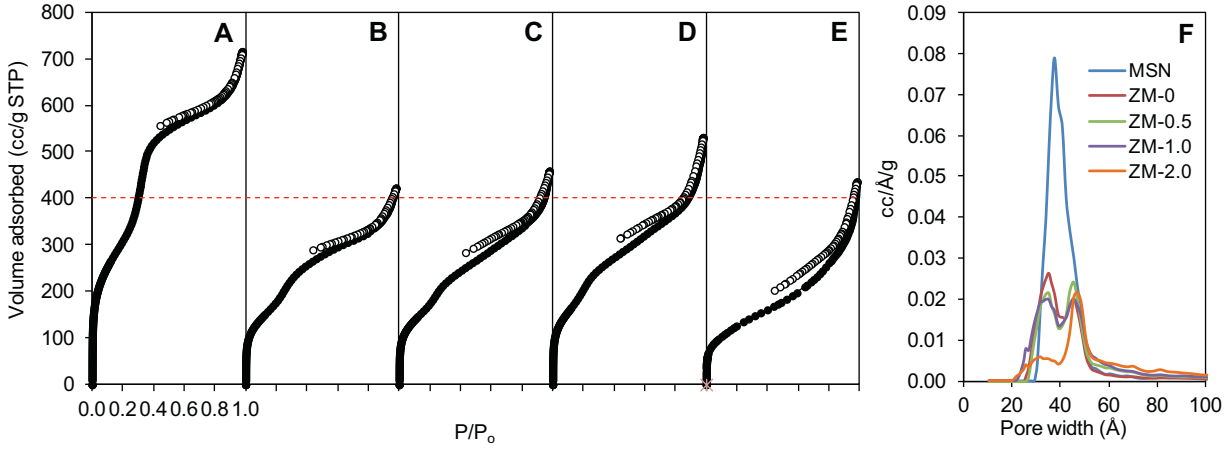

Fig. 4. N_2 adsorption–desorption isotherm plots of (A) MSN and ZM catalysts prepared by different amounts of NH_4OH (B) ZM-0 (C) ZM-0.5 (D) ZM-1.0 (E) ZM-2.0, and (F) NLDFT pore size distribution of MSN and ZM catalysts.

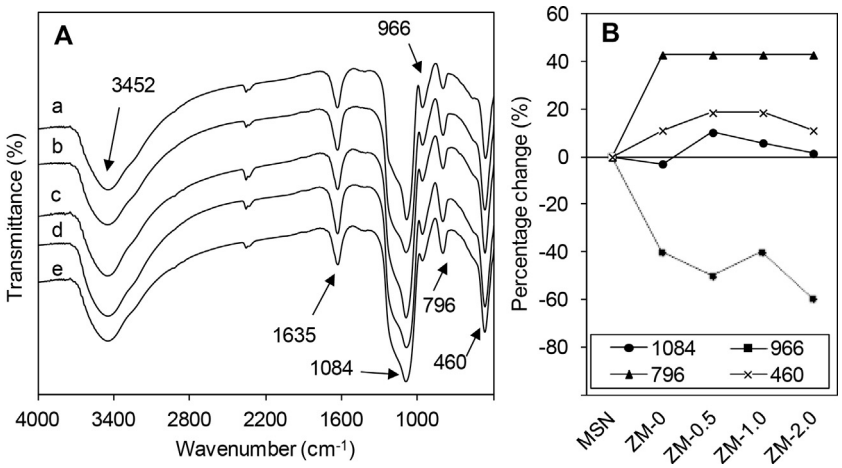

Fig. 5. (A) FTIR spectra of (a) MSN and ZM catalysts prepared by different amount of NH_4OH (b) ZM-0 (c) ZM-0.5 (d) ZM-1.0 and (e) ZM-2.0. (B) Percentage change of the related band compared to pure MSN band which calculated based on intensity of the band.

increased upon the introduction of Zn ions into the system, suggesting the calcination might dehydroxylyzed the unsubstituted silanol groups to form new Si–O–Si bonds [36]. The 796 cm^{-1} band remained unchanged upon the addition of NH_4OH solution, indicated that the Si–O–Si symmetric stretching band was not affected by the alkaline treatment. However, the Si–O–Si bending band at 460 cm^{-1} slightly increased for ZM-0.5. This may also be due to the formation of more Si–O–Si bonds as a result of additional desilication caused by the NH_4OH. In contrast, the Si–O–Si asymmetric stretching band at 1084 cm^{-1} decreased to some extent for the ZM-0 catalyst, representing the possible isomorphous substitution of Zn into the silica network. Both bands at 460 and 1084 cm^{-1} showed a similar trend of reduction upon the further addition of NH_4OH, particularly the latter, which confirmed that the desilication and/or isomorphous substitution were increased proportionately with the alkaline concentration. These results were in agreement with the pore size distribution shown in Fig. 4, indicating the intraparticle pore blockage effect on the increasing amount of NH_4OH, thus signifying the possible insertion of Zn into the pore of the MSN. The (1 0 0) peak in XRD diffractogram, which became lower in intensity by the increasing alkaline solution, also supported these results (Fig. 1). By comparing the three Si–O–Si bands, we concluded that the desilication or/and substitution of Si with Zn ions seem favor to be occurred at Si–O–Si asymmetric stretching band. Notably, the external Si–OH groups at band 966 cm^{-1} were drastically reduced by the addition of Zn or NH_4OH, illustrating that the insertion of Zn ions and/or desilication most readily occurred on the external surface of the MSN. It was also seen that the silanol groups of ZM-1.0 were slightly increased, which in parallel with the XRD and surface area analysis results, indicating the restructure enhancement of the catalyst under this condition.

Next, in order to determine the actual structure of ZM catalysts, the uncertain Si–O–H band at 966 cm^{-1} was further confirmed by a Gaussian curve-fitting (Fig. S1). For comparison of the band changes, an estimation was made based on the height bands intensity by considering all bands have a similar pattern. The results are listed in the inset table in Fig. S1. For the bare MSN (Fig. S1A), two bands were convoluted at 966 and 925 cm^{-1}, which correlate with the bending vibration of the Si–O–H groups. The band at 966 cm^{-1} were slightly shifted to a lower frequency (962 cm^{-1}) for the ZM-0 catalyst, while both bands seemed to have decreased intensity when Zn was introduced to the system (Fig. S1B). Accordingly, a new band emerged at 906 cm^{-1}, which likely resulted from the formation of the Si–O–Zn band [37]. We found that the addition of NH_4OH further reduced the Si–O–H groups while retaining the number Si–O–Zn bonds (Fig. S1C). However, the Si–OH groups, as well as Si–O–Zn bonds, seemed significantly increased when 1.0 M NH_4OH was added, confirming the increased desilication and formation of Si–O–Zn bonds under this condition (Fig. S1D). This result is also in agreement with the XRD and surface area analysis results. Although the exact reason is currently unclear, the 1.0 M NH_4OH was determined to be the best concentration for producing the 5 wt% ZnO/MSN catalyst with improved hierarchical-like silica arrangement and rich with Si–O–Si, Si–O–H and Si–O–Zn bonds, as evidenced by the above characterization data. Similar results were reported by Mokrzycki et al. for the synthesis of a ZSM-12-type zeolite via desilication process. They reported that the best structure was obtained upon increasing the NaOH concentration up to 0.5 M, which led to the highest catalytic activity when compared to other NaOH concentrations (0.1 and 1.0 M) [38]. Further addition of NH_4OH up to 2.0 M seemed to decrease the intensity of all the three peaks, supporting the pore distribution result which suggested the pore collapse as a consequence of treatment in higher alkaline concentration.

The MSN and ZM catalysts were also evacuated at 623 K for 1 h prior to IR measurements to remove the physisorbed water and the spectra are shown in Fig. S2. The sole sharp band at 3740 cm^{-1} corresponded to terminal groups located on the external surface of the MSN framework [39]. This band decreased in intensity and slightly shifted to a lower frequency when compared to the parent MSN when Zn and NH_4OH were added to the system. This also confirmed the perturbation of the external –OH groups for the formation of Si–O–Zn and/or new Si–O–Si bonds [30]. In addition, a new broad shouldered band was also observed at 3590–3480 cm^{-1}, which was assigned to the presence of $Si(OH)_4$ that resulted as a consequence of desilication in the MSN framework [40]. Baseline correction of the corresponding band revealed the presence of a broad band, especially for ZM-0 (Fig. S2B/b). However, this band decreased in intensity by increasing the NH_4OH concentration, with ZM-1.0 showing the lowest peak when compared to the others. This result also supported the restructuring of the MSN framework either by the formation of Si–O–Zn or new Si–O–Si bonds.

3.1.5. *Proposed structure of the ZM catalyst*

Based on the above characterization data, a probable mechanism for the formation of the ZM catalyst structure is illustrated in Fig. 6. The presence of TEAP, as well as NH_4OH, in the electrolysis cell allowed the desilication to occur, thus producing the hierarchical-like structure of MSN with abundant silanol nests on the surface of the silica framework [40]. The decrease in numbers of

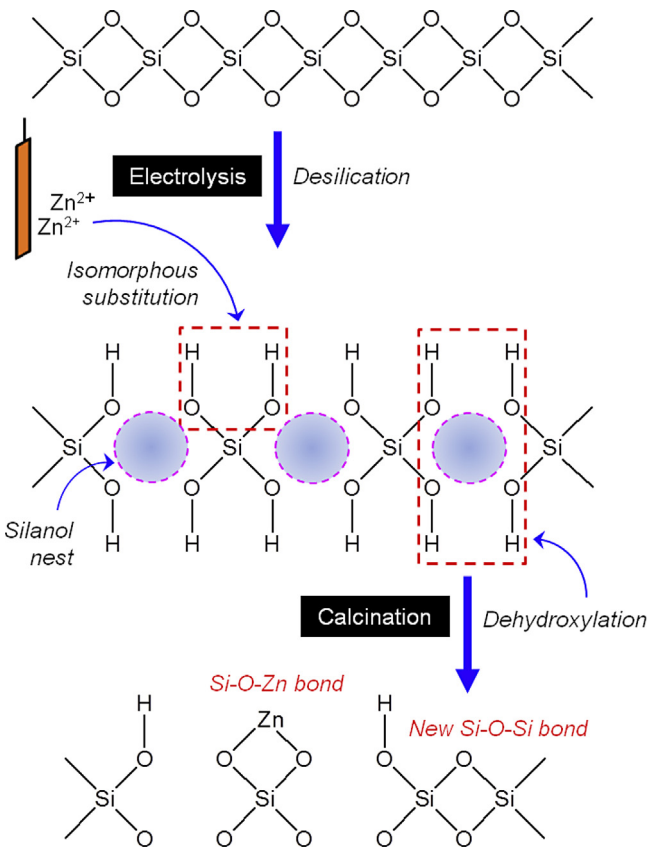

Fig. 6. Proposed structure of ZM catalysts.

external –OH groups signified the subsequent insertion of Zn cations to form Si–O–Zn bonds. In fact, our previous study confirmed that the isomorphous substitution was occurred during the electrolysis because the formation of Si–O–Fe bonds could not be traced when the electrolyzed Fe^{3+} ions was impregnated with HY zeolite after the electrolysis [21]. The remaining silanol groups were then produced new Si–O–Si bonds as a consequence of dehydroxylation during the calcination at 873 K [36]. The degree of desilication increased proportionally to some extent by the amount of NH_4OH added and affected the hierarchical-like structure. It is believed that this will lead to different capacities of Si–O–Zn and Si–O–Si bonds, as well as oxygen vacancies, which affects the photoactivity of the ZM catalysts.

3.2. Evaluation of photocatalytic activity

The photocatalytic behavior of the catalysts was evaluated based on their decolorization of methyl orange (MO), and the results are shown in Fig. 7A. A control experiment conducted in the presence of the bare MSN showed that no significant decolorization was achieved after 8 h. However, the addition of 5 wt% ZnO into the system (ZM-0) clearly increased the initial decolorization rate up to 6.52×10^{-3} mM h^{-1} proving the important role of ZnO in the reaction. Varying the amount of NH_4OH revealed the photocatalytic efficiency in the following order: ZM-1.0 (11.8×10^{-3} mM h^{-1}) > ZM-0.5 (8.69×10^{-3} mM h^{-1}) > ZM-2.0 (4.54×10^{-3} mM h^{-1}).

It was reported that the different photocatalytic efficiencies were most likely due to the influence of the hierarchical porous silica arrangements of the catalysts [41]. In order to confirm this, the catalysts were subjected to photoluminescence (PL) analysis (Fig. 7B). The three catalysts (ZM-0, ZM-1.0 and ZM-2.0) showed similar spectra trends, which consisted of two main parts: the first was near the ultraviolet region and the second was an intense defect-related band in the visible light region. It is well known that the green-yellow emission band around 480–650 nm originated from defect emission associated with oxygen vacancies [42]. The larger content of oxygen vacancies or defects in the catalyst lead to the stronger PL signals in this band. It was also reported that the oxygen vacancies can become the centers that capture photoinduced electrons during the photocatalytic reaction, which inhibited the recombination of photoinduced charge carriers and lead to the higher photoactivity of the catalyst [43]. Moreover, oxygen vacancies could also promote the adsorption of O_2, which also plays an important role in promoting the oxidation of organic dye pollutants. Thus, it is possible that the largest number of oxygen vacancies of ZM-1.0 was the main reason for its higher photoactivity when compared to other catalysts studied. A similar study was also reported by Wang et al. for the synthesis of ZnO using different annealing temperatures. They reported that a low annealing temperature produce high oxygen vacancies in the ZnO samples, thus leading to higher photocatalytic activity [44]. Accordingly, the more desilication that occurred resulted in the greater formation of oxygen vacancies, which then led to the higher photoactivity of the ZM-1.0, as confirmed by the XRD, FTIR, and surface area analyses.

3.2.1. Kinetic studies

To study the kinetics of MO decolorization, a linear fitting of $\ln(C_0/C_t)$ *versus* irradiation time (t) over the ZM catalysts was plotted (Fig. 7C). The linearity of the curves for all the catalysts reveals that the photodecolorization process follows first order reaction kinetics and the rate expression is given as follows,

$$-\frac{d[C]}{dt} = kC \tag{2}$$

where k is the pseudo-first order rate constant. With the limit of $C = C_0$ at $t = 0$, with C_0 being the equilibrium concentration of the bulk solution, an integration of the Eq. (2) gave Eq. (3),

$$\ln \frac{C_0}{C_t} = kt \tag{3}$$

where C_t is the MO concentration at time t. The slope of the line is the first-order rate constant (k_a) and the calculated values were to be 3.87×10^{-1}, 2.85×10^{-1}, 2.14×10^{-1}, 1.49×10^{-1} h^{-1}, and 0.13×10^{-1} h^{-1} for ZM-1.0, ZM-0.5, ZM-0, ZM-2.0, and MSN, respectively (Table 1). These results provided further verification supporting the efficiency of the ZM-1.0 compared to the other ZM catalysts. In addition, a higher rate was obtained for all ZM catalysts, displaying an increased activity compared to the unsupported ZnO (1.13×10^{-1} h^{-1}) that prepared under the same conditions in the absence of MSN (figure not shown).

The k_a was also normalized by the surface area in order to determine the effect of surface area of the catalysts on the photocatalytic activity (Table 1). It was found that the order of normalized rate constant k_b was similar to the k_a, verifying the photocatalytic activity of the catalysts was not influenced by the surface area but was most probably due to the effect of the recombination rate of photoinduced electron–hole pairs [45]. This result also supports the enhanced ZM-1.0 photoactivity due to its higher number of oxygen vacancies as compared to other catalysts that acted as electrons acceptor for enhanced electron–hole separation.

3.2.2. Proposed photodecolorization mechanism

Accordingly, the ZM-1.0 catalyst was chosen for further investigation of the mechanism of MO decolorization. Four scavenging agents were used in order to identify the key factor in the reaction: isopropanol (IP), sodium oxalate (SO), benzyl chloride (BC), and kalium iodide (KI), which act as a hydroxyl radical scavenger (•OH), hole capturer (h^+), electron trapper (e^-), and surface hydroxyl

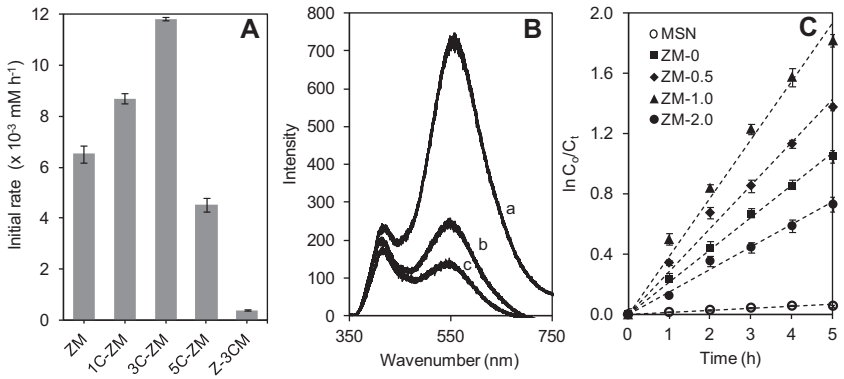

Fig. 7. (A) Performance of catalysts on photodecolorization of MO (B) photoluminescence analysis of (a) ZM-1.0, (b) ZM-0 and (c) ZM-2.0, and (C) kinetics studies of MO photodecolorization.

radical scavenger ($^{\bullet}OH_{ad}$), respectively. Comparing the decolorization rate in the absence of a scavenger, the KI slightly inhibited the initial reaction rate (Fig. 8A). In comparison, the decolorization rate was reduced by half with the addition of SO or BC. However, a greater inhibition of photocatalytic activity was observed using IP, confirming the significant role of the hydroxyl radical $^{\bullet}OH$ in the system. Based on these results, a mechanism for the photodecolorization is proposed as follows (Fig. 8B), an irradiation of the ZM catalyst generated an electron–hole pair,

$$ZM + h\nu \rightarrow e^- + h^+ \quad (4)$$

The electrons at the conduction band were highly potential and negative enough to reduce O_2 to ensure the formation of superoxide radical $^{\bullet}O_2^-$, which was subsequently reduced to form H_2O_2 and $^{\bullet}OH$ [46],

$$O_2 + e^- \rightarrow {}^{\bullet}O_2^- \quad (5)$$

$$^{\bullet}O_2^- + e^- + 2H^+ \rightarrow H_2O_2 \quad (6)$$

$$H_2O_2 + e^- \rightarrow OH^- + {}^{\bullet}OH \quad (7)$$

The positively charged hole (h^+) at valence band was also responsible for the production of free $^{\bullet}OH$,

$$H_2O + h^+ \rightarrow {}^{\bullet}OH + H^+ \quad (8)$$

In addition, UV-light irradiation also reduced the H_2O_2 present in the solution to form free $^{\bullet}OH$,

$$H_2O_2 \xrightarrow{h\nu} 2\,{}^{\bullet}OH \quad (9)$$

Therefore, it was anticipated that, due to the abundant $^{\bullet}OH$ generated from the three main sources that it plays an important role in the reaction. Similar results were previously reported in the literature, and described that $^{\bullet}OH$ plays an important role in the photooxidation of As(III) over natural montmorillonite catalyst [47].

3.2.3. Stability and reusability study

The potential of catalyst to be recovered and reused in photocatalytic processes is a great concern since it can contribute to lower the operational cost of processes, thus bring the photocatalysis toward an attractive method for wastewater treatment [48]. Hence, a repeated experiment was carried out using ZM-1.0 catalyst in order to study the stability of the catalyst for MO decolorization (Fig. 9). The initial concentration of MO was kept constant (3.06×10^{-2} mM) at pH 2 and 8 h of irradiation time, and the catalyst was recycled after filtration and calcination at 823 K for 3 h at every cycle. It can be observed that after five repeated experiments, the catalyst was still active with just small decreases in the initial rate from 11.8×10^{-3} mM h^{-1} to 10.5×10^{-3} mM h^{-1}. The results suggest that formation of Si–O–Zn bond plays an important role in the photocatalytic reaction.

To verify the results, the effect of zinc leaching into the solution was studied. The sample was kept in dark for 1 h and then irradiated under UV light for 8 h using an amount of 1 g L^{-1} ZM-1.0 catalyst in 3.06×10^{-2} mM MO solution at pH 2. The samples then were subjected to microwave plasma-atomic emission spectrometer (MP-AES). The amount of zinc detected in the solution

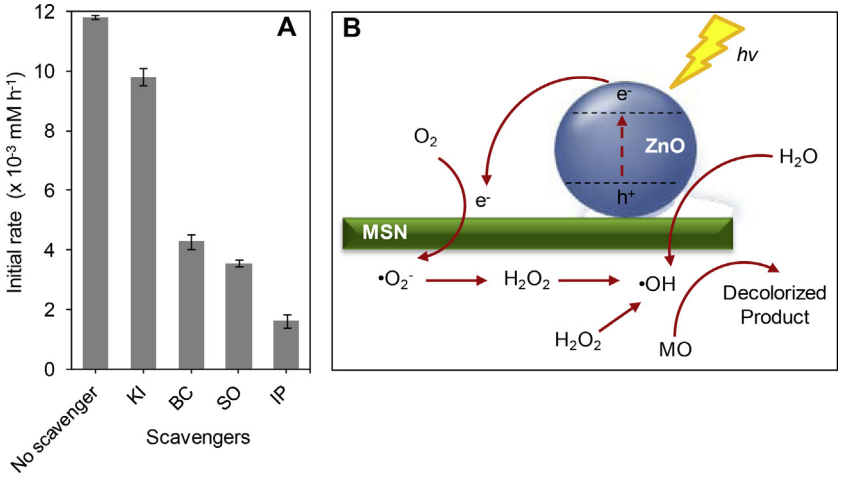

Fig. 8. (A) Photodecolorization efficiencies of MO in the presence of scavengers (B) proposed mechanism for photodecolorization of MO over ZM-1.0 catalyst.

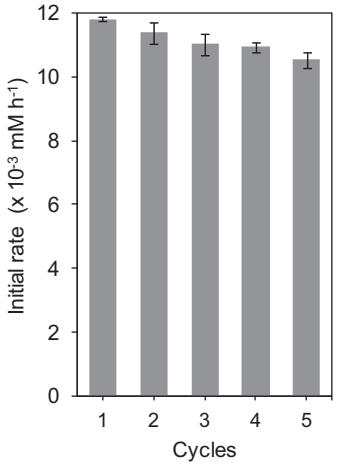

Fig. 9. Reusability of ZM-1.0 catalyst on photodecolorization of MO.

was less than 1.68×10^{-2} mM (<2.3%). Only a small amount of zinc was leached, signifying the zinc present on the catalyst surface (Si–O–Zn) preserved the stability and efficiency of the catalyst in the photocatalytic reaction. The similar result was also observed by Mahesh et al., which proved the formation of chemical bonding between SiO_2/TiO_2 composites and polyurethane had avoid the leaching of SiO_2/TiO_2 composite during photocatalytic degradation of acid black 1 (AB 1) [49].

4. Conclusion

In this study, a simple electrochemical method was applied to prepare ZnO-incorporated mesostructured silica nanoparticles (ZM) catalysts with hierarchical-like structure. The physicochemical properties of the synthesized catalysts were studied by XRD, ^{29}Si MAS NMR, nitrogen adsorption–desorption, FE-SEM, TEM, FTIR, and PL spectroscopy. We found that the TEAP and NH_4OH play important roles in the desilication in the MSN framework to form abundant silanol nests that created the hierarchical-like structure. Subsequent insertion of Zn ions, which were generated from dissolution at the anode into the external hydroxyl groups of MSN, formed Si–O–Zn bonds that improved the arrangement of the silica network. The degree of the desilication in forming the hierarchical-like structure could be controlled by the concentration of the NH_4OH solution. The more desilication occurred, the greater the formation of oxygen vacancies, which then led to enhanced electron–hole separation. Therefore, the ZM-1.0 was found to be the most effective catalyst due to its improved structure and higher oxygen vacancies, which facilitate the photodecolorization of MO dye. The experiment on effect of scavengers showed that hydroxyl radicals generated from the three main sources; reduced O_2 at the conduction band, decomposed water at the valence band and irradiated H_2O_2 in the solution, are key factors that influenced the reaction. The kinetic study showed that the decolorization process followed first-order kinetics, with a reaction rate of 3.87×10^{-1} h^{-1}. Less than 2.3% Zn was detected to be leached from the ZM-1.0 catalyst during the photocatalytic reaction and its ability to maintain the activity up to five runs without serious catalyst deactivation indicated its potential to be used as a promising catalyst in wastewater treatment.

Acknowledgments

The authors are grateful for the financial support by the Fundamental Research Grant Scheme (Grant No. 4F423) and the awards of MyPhD Scholarship (Nurfatehah Wahyuny Che Jusoh) from the Ministry of Higher Education. The authors also thankful to the Hitachi Scholarship Foundation for their support and the NANO-SciTech Centre of Universiti Teknologi Mara for the PL instrument.

Appendix A. Supplementary data

Supplementary data associated with this article can be found, in the online version, at http://dx.doi.org/10.1016/j.apsusc.2014.12.192.

References

[1] Q. Liu, J. Yang, X. Sun, X. Cheng, H. Tang, H. Li, Influence of W doped ZrV2O7 on structure, negative thermal expansion property and photocatalytic performance, Appl. Surf. Sci. 313 (2014) 41–47.
[2] S. Zhu, F. Yao, C. Yin, Y. Li, W. Peng, J. Ma, D. Zhang, Fe2O3/TiO2 photocatalyst of hierarchical structure for H2 production from water under visible light irradiation, Micropor. Mesopor. Mat. 190 (2014) 10–16.
[3] R.Y. Hong, J.H. Li, L.L. Chen, D.Q. Liu, H.Z. Li, Y. Zheng, J. Ding, Synthesis, surface modification and photocatalytic property of ZnO nanoparticles, Powder Technol. 189 (2009) 426–432.
[4] Y. Wang, S. Zhu, X. Chen, Y. Tang, Y. Jiang, Z. Peng, H. Wang, One-step template-free fabrication of mesoporous ZnO/TiO2 hollow microspheres with enhanced photocatalytic activity, Appl. Surf. Sci. 307 (2014) 263–271.
[5] J. Xie, H. Wang, M. Duan, L. Zhang, Synthesis and photocatalysis properties of ZnO structures with different morphologies via hydrothermal method, Appl. Surf. Sci. 257 (2011) 6358–6363.
[6] J. Zhuang, W. Dai, Q. Tian, Z. Li, L. Xie, J. Wang, P. Liu, X. Shi, D. Wang, Photocatalytic degradation of RhB over TiO2 bilayer films: effect of defects and their location, Langmuir 26 (2010) 9686–9694.
[7] G.D. Mihai, V. Meynen, M. Mertens, N. Bilba, P. Cool, E.F. Vansant, ZnO nanoparticles supported on mesoporous MCM-41 and SBA-15: a comparative physicochemical and photocatalytic study, J. Mater. Sci. 45 (2010) 5786–5794.
[8] N.H.N. Kamarudin, A.A. Jalil, S. Triwahyono, V. Artika, N.F.M. Salleh, A.H. Karim, N.F. Jaafar, M.R. Sazegar, R.R. Mukti, B.H. Hameed, A. Johari, Variation of the crystal growth of mesoporous silica nanoparticles and the evaluation to ibuprofen loading and release, J. Colloid Interface Sci. 421 (2014) 6–13.
[9] M.A.A. Aziz, A.A. Jalil, S. Triwahyono, R.R. Mukti, Y.H. Taufiq-Yap, M.R. Sazegar, Highly active Ni-promoted mesostructured silica nanoparticles for CO2 methanation, Appl. Catal. B: Environ. 147 (2014) 359–368.
[10] M.R. Sazegar, A.A. Jalil, S. Triwahyono, R.R. Mukti, M. Aziz, M.A.A. Aziz, H.D. Setiabudi, N.H.N. Kamarudin, Protonation of Al-grafted mesostructured silica nanoparticles (MSN): acidity and catalytic activity for cumene conversion, Chem. Eng. J. 240 (2014) 352–361.
[11] A.H. Karim, A.A. Jalil, S. Triwahyono, N.H.N. Kamarudin, A. Ripin, Influence of multi-walled carbon nanotubes on textural and adsorption characteristics of in situ synthesized mesostructured silica, J. Colloid Interface Sci. 421 (2014) 93–102.
[12] S. Tao, Y. Wang, Y. Yu, Y. An, W. Shi, Hierarchically porous tungstophosphoric acid/silica hybrid for high performance vis-light photocatalysis, J. Environ. Chem. Eng. 1 (2013) 719–727.
[13] J.C. Groen, S. Abelló, L.A. Villaescusa, J. Pérez-Ramírez, Mesoporous beta zeolite obtained by desilication, Micropor. Mesopor. Mat. 114 (2008) 93–102.
[14] Z. Miao, S. Tao, Y. Wang, Y. Yu, C. Meng, Y. An, Hierarchically porous silica as an efficient catalyst carrier for high performance vis-light assisted Fenton degradation, Micropor. Mesopor. Mat. 176 (2013) 178–218.
[15] M. Ogura, S.-y. Shinomiya, J. Tateno, Y. Nara, M. Nomura, E. Kikuchi, M. Matsukata, Alkali-treatment technique – new method for modification of structural and acid-catalytic properties of ZSM-5 zeolites, Appl. Catal. A: Gen. 219 (2001) 33–43.
[16] A. Čižmek, B. Subotić, R. Aiello, F. Crea, A. Nastro, C. Tuoto, Dissolution of high-silica zeolites in alkaline solutions I. Dissolution of silicalite-1 and ZSM-5 with different aluminum content, Microporous Mater. 4 (1995) 159–168.
[17] A. Čižmek, B. Subotić, I. Šmit, A. Tonejc, R. Aiello, F. Crea, A. Nastro, Dissolution of high-silica zeolites in alkaline solutions II. Dissolution of 'activated' silicalite-1 and ZSM-5 with different aluminum content, Microporous Mater. 8 (1997) 159–169.
[18] S. Abelló, A. Bonilla, J. Pérez-Ramírez, Mesoporous ZSM-5 zeolite catalysts prepared by desilication with organic hydroxides and comparison with NaOH leaching, Appl. Catal. A: Gen. 364 (2009) 191–198.
[19] M. Pimsuta, A. Neramittagapong, S. Prayoonpokarach, J. Wittayakun, Desilication of NaZSM-5 and utilization as support of Fe for phenol hydroxylation, Int. J. Chem. Eng. Appl. 3 (2012) 86–91.
[20] N. Sapawe, A.A. Jalil, S. Triwahyono, One-pot electro-synthesis of ZrO2–ZnO/HY nanocomposite for photocatalytic decolorization of various dye-contaminants, Chem. Eng. J. 225 (2013) 254–265.
[21] N.F. Jaafar, A. Abdul Jalil, S. Triwahyono, M.N. Muhd Muhid, N. Sapawe, M.A.H. Satar, H. Asaari, Photodecolorization of methyl orange over α-Fe2O3-supported HY catalysts: the effects of catalyst preparation and dealumination, Chem. Eng. J. 191 (2012) 112–122.
[22] N.W.C. Jusoh, A.A. Jalil, S. Triwahyono, H.D. Setiabudi, N. Sapawe, M.A.H. Satar, A.H. Karim, N.H.N. Kamarudin, R. Jusoh, N.F. Jaafar, N. Salamun, J. Efendi,

Sequential desilication–isomorphous substitution route to prepare mesostructured silica nanoparticles loaded with ZnO and their photocatalytic activity, Appl. Catal. A: Gen. 468 (2013) 276–287.
[23] S. Krijnen, Titanium Epoxidation Catalysts: Zeolite and Silsesquioxane based Material, Technische Universiteit Eindhoven, Eindhoven, 1998.
[24] A.A. Jalil, N. Fatimah, A. Panjang, S. Akhbar, M. Sundang, N. Tajuddin, S. Triwahyono, Complete electrochemical dechlorination of chlorobenzenes in the presence of naphthalene mediator, J. Hazard. Mater. 148 (2007) 1–5.
[25] A.A. Jalil, N. Kurono, M. Tokuda, Facile synthesis of 2-arylpropenoic acid esters by cross-coupling using electrogenerated highly reactive zinc and a palladium catalyst, Synlett 12 (2001) 1944–1946.
[26] A.A. Jalil, N. Kurono, M. Tokuda, Synthesis of the precursor of anti-inflammatory agents by cross-coupling using electrogenerated highly reactive zinc, Synthesis 18 (2002) 2681–2686.
[27] M.S. Holm, S. Svelle, F. Joensen, P. Beato, C.H. Christensen, S. Bordiga, M. Bjørgen, Assessing the acid properties of desilicated ZSM-5 by FTIR using CO and 2,4,6-trimethylpyridine (collidine) as molecular probes, Appl. Catal. A: Gen. 356 (2009) 23–30.
[28] Y. Li, N. Li, J. Tu, X. Li, B. Wang, Y. Chi, D. Liu, D. Yang, TiO2 supported on rod-like mesoporous silica SBA-15: preparation, characterization and photocatalytic behaviour, Mater. Res. Bull. 46 (2011) 2317–2322.
[29] C. Wu, Y. Kong, F. Gao, Y. Wu, Y. Lu, J. Wang, L. Dong, Synthesis, characterization and catalytic performance for phenol hydroxylation of Fe-MCM41 with high iron content, Micropor. Mesopor. Mat. 113 (2008) 163–170.
[30] P.B. Lihitkar, S. Violet, M. Shirolkar, J. Singh, O.N. Srivastava, R.H. Naik, S.K. Kulkarni, Confinement of zinc oxide nanoparticles in ordered mesoporous silica MCM-41, Mater. Chem. Phys. 133 (2012) 850–856.
[31] X.W. Cheng, Q.Y. Meng, J.Y. Chen, Y.C. Long, A facile route to synthesize mesoporous ZSM-5 zeolite incorporating high ZnO loading in mesopores, Micropor. Mesopor. Mat. 153 (2012) 198–203.
[32] W. Lu, G. Lu, Y. Luo, A. Chen, A novel preparation method of ZnO/MCM-41 for hydrogenation of methyl benzoate, J. Mol. Catal. A: Chem. 188 (2002) 225–231.
[33] E. Prouzet, F. Cot, G. Nabias, A. Larbot, P. Kooyman, T.J. Pinnavaia, Assembly of mesoporous silica molecular sieves based on nonionic ethoxylated sorbitan esters as structure directors, Chem. Mater. 11 (1999) 1498–1503.
[34] H. Mochizuki, T. Yokoi, H. Imai, S. Namba, J.N. Kondo, T. Tatsumi, Effect of desilication of H-ZSM-5 by alkali treatment on catalytic performance in hexane cracking, Appl. Catal. A: Gen. 449 (2012) 188–197.
[35] J. Li, X. Li, G. Zhou, W. Wang, C. Wang, S. Komarneni, Y. Wang, Catalytic fast pyrolysis of biomass with mesoporous ZSM-5 zeolites prepared by desilication with NaOH solutions, Appl. Catal. A: Gen. 470 (2014) 115–122.
[36] X.S. Zhao, G.Q. Lu, A.K. Whittaker, G.J. Millar, H.Y. Zhu, Comprehensive study of surface chemistry of MCM-41 using 29Si CP/MAS NMR, FTIR, Pyridine-TPD, and TGA, T. J. Phys. Chem. B 101 (1997) 6525–6531.
[37] J.W. Soares, J.E. Whitten, D.W. Oblas, D.M. Steeves, Novel photoluminescence properties of surface-modified nanocrystalline zinc oxide: toward a reactive scaffold, Langmuir 24 (2007) 371–374.
[38] Ł. Mokrzycki, B. Sulikowski, in: P.M. Antoine Gédéon, B. Florence (Eds.), Desilication of ZSM-12 and MCM-22 Type Zeolites and their Performance in Isomerization of α-Pinene, Elsevier, 2008, pp. 1231–1234.
[39] P. Hoffmann, J.A. Lobo, Identification of diverse silanols on protonated ZSM-5 zeolites by means of FTIR spectroscopy, Micropor. Mesopor. Mat. 106 (2007) 122–128.
[40] B. Gil, Ł. Mokrzycki, B. Sulikowski, Z. Olejniczak, S. Walas, Desilication of ZSM-5 and ZSM-12 zeolites: impact on textural, acidic and catalytic properties, Catal. Today 152 (2010) 24–32.
[41] B. Rohe, W.S. Veeman, M. Tausch, Synthesis photocatalytic activity of silane-coated and UV-modified nanoscale zinc oxide, Nanotechnology 17 (2006) 277.
[42] S.A. Ansari, M.M. Khan, S. Kalathil, A. Nisar, J. Lee, M.H. Cho, Oxygen vacancy induced band gap narrowing of ZnO nanostructures by an electrochemically active biofilm, Nanoscale 5 (2013) 9238–9246.
[43] L. Jing, F. Yuan, H. Hou, B. Xin, W. Cai, H. Fu, Relationships of surface oxygen vacancies with photoluminescence and photocatalytic performance of ZnO nanoparticles, Sc. China Ser. B-Chem. 48 (2005) 25–30.
[44] J. Wang, Z. Wang, B. Huang, Y. Ma, Y. Liu, X. Qin, X. Zhang, Y. Dai, Oxygen vacancy induced band-gap narrowing and enhanced visible light photocatalytic activity of ZnO, ACS Appl. Mater. Interfaces 4 (2012) 4024–4030.
[45] P. Gao, A. Li, D.D. Sun, W.J. Ng, Effects of various TiO2 nanostructures and graphene oxide on photocatalytic activity of TiO2, J. Hazard. Mater. 279 (2014) 96–104.
[46] Y. Wang, K. Deng, L. Zhang, Visible light photocatalysis of BiOI and its photocatalytic activity enhancement by in situ ionic liquid modification, T. J. Phys. Chem. C 115 (2011) 14300–14308.
[47] Y. Wang, J. Xu, J. Li, F. Wu, Natural montmorillonite induced photooxidation of As(III) in aqueous suspensions: roles and sources of hydroxyl and hydroperoxyl/superoxide radicals, J. Hazard. Mater. 260 (2013) 255–262.
[48] B. Barrocas, O.C. Monteiro, M.E.M. Jorge, S. Sério, Photocatalytic activity and reusability study of nanocrystalline TiO2 films prepared by sputtering technique, Appl. Surf. Sci. 264 (2013) 111–116.
[49] K.P.O. Mahesh, D.-H. Kuo, B.-R. Huang, M. Ujihara, T. Imae, Chemically modified polyurethane-SiO2/TiO2 hybrid composite film and its reusability for photocatalytic degradation of Acid Black 1 (AB 1) under UV light, Appl. Catal. A: Gen. 475 (2014) 235–241.